Discrete Orthogonal Decomposition and Variational Fluid Flow Estimation

Jing Yuan, Christoph Schnörr, Étienne Mémin

[1]University of Mannheim
CVGPR Group, Germany
{yuanjing,schnoerr}@uni-mannheim.de

[1]INRIA/IRISA Rennes
VISTA Group, France
Etienne.Memin@irisa.fr

Abstract

We exploit the mimetic finite difference method introduced by Hyman and Shashkov to present a framework for estimating vector fields and related scalar fields (divergence, curl) of physical interest from image sequences. Our approach provides a basis for consistent definitions of higher-order differential operators, for the analysis and a novel stability result concerning second-order div-curl regularizers, for novel variational schemes to the estimation of solenoidal (divergence-free) image flows, and to convergent numerical methods in terms of subspace corrections.

1 Introduction

The estimation of highly non-rigid image flows is an important problem in various application areas of image analysis like remote sensing, medical imaging, and experimental fluid mechanics. Such flows, which cannot be represented by a single parametric model, are typically estimated by variational approaches. In contrast to standard approaches, however, higher-order regularization is necessary in order to accurately recover important flow structures like vortices, for example, and to incorporate physically plausible constraints, like vanishing divergence of the flow.

The basis for our paper is early work on second-order regularizers constraining the gradients of the flow components divergence and curl [1, 17, 10]. This regularization approach has been elaborated in a series of papers by Mémin and co-workers [7, 8]. Moreover, the decomposition and representation of *continuous* vector fields by velocity potentials and stream functions [9] has been adopted to derive piecewise parametric representations of relevant flow structures. Recently, the direct estimation of this representation from image sequences has been studied in [14].

The objective of this contribution is to provide a mathematically sound discrete representation of vector fields in terms of basic flow components related to quantities of physical relevance, and a correponding decomposition into subspaces of the linear space of discrete vector valued functions. By this, we obtain and can investigate a discrete analogue of known continuous representations [9] in connection with image sequence analysis of fluids. This gives

rise, for example, to a novel variational approach for estimation solenoidal (divergence-free) flows from image sequences. Furthermore, we remove numerical convergence problems of the heuristic alternating numerical estimation scheme employed in [14] by adopting a subspace correction method from numerical analysis which directly applies to our flow field representation. Finally, our analysis reveals the importance of an additional boundary regularization term in connection div-curl regularizers (section 4.3), which has been overlooked apparently in previous work.

In section 2, we present the discrete representation of both scalar and vector fields based on the mimetic finite difference method introduced by Hyman and Shashkov [12, 11]. A basic feature of this representation is that basic integral identities of vector analysis are preserved after discretization. Furthermore, basic first-order differential operators can be defined such that compound higher-order operators with compatible domains and image spaces can be consistently defined. Subsequently, we elaborate the representation of vector fields by potential and stream functions and various useful subspace decompositions of the linear space of discrete vector fields.

Based on this, we reconsider a few variational approaches to motion estimation in section 3. By defining all quantities in terms of the representation developed in section 2, we examine well-posedness and stability, including the non-trivial stability issue mentioned above (section 4). Section 5 provides a natural numerical estimation approach which directly fits to the flow field representation, along with details of the multilevel implementation. We validate our approach with numerical experiments in section 6.

A preliminary conference version of this paper appeared in [25].

2 Vector-Field Representation

2.1 Discrete Fields and Differential Operators

We use the *mimetic finite difference method* introduced by Hyman and Shashkov [12, 11] in order to preserve basic relationships of continuous vector analysis by appropriately defining their discrete analogues. This discretization scheme will be applied in section 2.2 to accurately represent and decompose vector fields.

Linear Spaces. Figure 1 illustrates the definitions of the following finite-dimensional vector spaces of scalar and vector fields that naturally appear in discrete models of continuum mechanics:

- H_V: the space of *scalar fields* defined on cells,
- H_P: the space of *scalar fields* defined on vertices,
- H_E: the space of *vector fields* defined tangential to sides,
- H_S: the space of *vector fields* defined normal to sides.

We denote with H_P^o, H_S^o, H_E^o the subspaces of inner scalar and inner vector fields, respectively, obtained by restricting the spaces H_P^o, H_S^o, H_E^o, and by imposing zero boundary values.

Notation. We denote with $L_{i,j+1/2}$ the side between vertices (i,j) and $(i,j+1)$. The relationship between vertex indices and cell indices is depicted in Figure 1 for the lower-right cell, denoted with $\Omega_{i+1/2,j+1/2}$. To simplify notation, we index cell (side, vertex) positions sometimes directly with (α,β) if the meaning is unambiguous. Ω denotes the whole image section, and $\partial\Omega$ its boundary,

Convention. We consider in this paper only regular grids with unit side-lengths $L_{\alpha,\beta} = 1$ and unit cell-areas $\Omega_{\alpha,\beta} = 1\,,\ \forall\alpha,\beta$. Let our grid consist of $m \times n$ vertices. Reshaping the scalar/vector fields columnwise into vectors, we identify: $H_P = \mathbb{R}^{mn},\ H_P^o = \mathbb{R}^{(m-2)(n-2)}, H_V = \mathbb{R}^{(m-1)(n-1)},\ H_S = \mathbb{R}^{m(n-1)+n(m-1)}, H_S^o = \mathbb{R}^{(m-1)(n-2)+(n-1)(m-2)}$, and H_E, H_E^o with H_S, H_S^o.

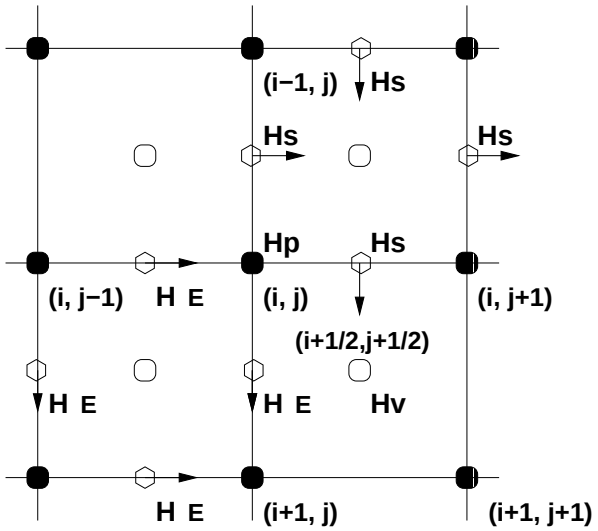

Figure 1: Definition of finite-dimensional spaces of scalar fields and vector fields on a rectangular grid. Filled circles depict *nodes* or *vertices*, the other circles indicate *cells*. The positions of diamonds are referred to as *sides*.

Inner products and Norms. While H_P and H_V are equipped with the usual euclidian inner product

$$\langle g,h\rangle_{H_V} = \sum_{\Omega_{\alpha,\beta}\in\Omega} g_{\alpha,\beta}h_{\alpha,\beta}\ ,$$

and with the corresponding induced norm, the inner products on H_S and H_E are defined as follows: let the indices D,T,R,L refer to the sides of cell $\Omega_{\alpha,\beta}$, $u \in H_S$, and

$$u_{\Omega_{\alpha,\beta}} := \frac{1}{\sqrt{2}}\,(u_D,u_T,u_R,u_L)^{\mathrm{T}}_{\alpha,\beta}\ .$$

Then

$$\langle u,v\rangle_{H_S} := \sum_{\Omega_{\alpha,\beta}\in\Omega} \langle u_{\Omega_{\alpha,\beta}}, v_{\Omega_{\alpha,\beta}}\rangle\ , \quad \|u\|_{H_S} := \sqrt{\langle u,u\rangle_{H_S}}\ .$$

Analogous definitions hold for H_E.

First-order Differential Operators. We define the discrete first-order differential operators corresponding to ∇, $\nabla^\perp$, div, and curl, operating on discretized 2D data:

$$\mathbb{G} : H_P \to H_E,\ \mathbb{G}^\perp : H_P \to H_S,\ \mathbb{D}iv\ : H_S \to H_V,\ \mathbb{C}url\ : H_E \to H_V, \tag{1a}$$

$$\overline{\mathbb{G}} : H_{V+\partial V} \to H_S,\ \overline{\mathbb{G}}^\perp : H_{V+\partial V} \to H_E,\ \overline{\mathbb{D}iv}\ : H_E^o \to H_P^o,\ \overline{\mathbb{C}url}\ : H_S^o \to H_P^o. \tag{1b}$$

Let

$$\boldsymbol{D}_m := \begin{pmatrix} -1 & 1 & 0 & \dots & 0 & 0 & 0 \\ 0 & -1 & 1 & \dots & 0 & 0 & 0 \\ & & \ddots & \ddots & \ddots & & \\ 0 & 0 & 0 & \dots & -1 & 1 & 0 \\ 0 & 0 & 0 & \dots & 0 & -1 & 1 \end{pmatrix} \in \mathbb{R}^{m-1,m},$$

and

$$\tilde{\boldsymbol{D}}_m := \begin{pmatrix} -2 & 2 & 0 & 0 & \dots & 0 & 0 & 0 & 0 \\ 0 & -1 & 1 & 0 & \dots & 0 & 0 & 0 & 0 \\ 0 & 0 & -1 & 1 & \dots & 0 & 0 & 0 & 0 \\ & & & \ddots & \ddots & \ddots & & & \\ 0 & 0 & 0 & 0 & \dots & -1 & 1 & 0 & 0 \\ 0 & 0 & 0 & 0 & \dots & 0 & -1 & 1 & 0 \\ 0 & 0 & 0 & 0 & \dots & 0 & 0 & -2 & 2 \end{pmatrix} \in \mathbb{R}^{m,m+1}.$$

Then the discrete operators are represented by the following matrices

$$\begin{aligned} \mathbb{G} &= \begin{pmatrix} \boldsymbol{I}_n \otimes \boldsymbol{D}_m \\ \boldsymbol{D}_n \otimes \boldsymbol{I}_m \end{pmatrix}, \quad \overline{\mathbb{G}} = \begin{pmatrix} \boldsymbol{I}_{n-1} \otimes \tilde{\boldsymbol{D}}_m \\ \tilde{\boldsymbol{D}}_n \otimes \boldsymbol{I}_{m-1} \end{pmatrix}, \\ \mathbb{D}iv &= \begin{pmatrix} \boldsymbol{I}_{n-1} \otimes \boldsymbol{D}_m, \boldsymbol{D}_n \otimes \boldsymbol{I}_{m-1} \end{pmatrix}, \\ \overline{\mathbb{D}iv} &= \begin{pmatrix} \boldsymbol{I}_{n-2} \otimes \boldsymbol{D}_{m-1}, \boldsymbol{D}_{n-1} \otimes \boldsymbol{I}_{m-2} \end{pmatrix}, \\ \mathbb{C}url &= \begin{pmatrix} \boldsymbol{D}_n \otimes \boldsymbol{I}_{m-1}, -\boldsymbol{I}_{n-1} \otimes \boldsymbol{D}_m \end{pmatrix}, \\ \overline{\mathbb{C}url} &= \begin{pmatrix} \boldsymbol{D}_{n-1} \otimes \boldsymbol{I}_{m-2}, -\boldsymbol{I}_{n-2} \otimes \boldsymbol{D}_{m-1} \end{pmatrix}, \end{aligned}$$

where $\otimes$ denotes the Kronecker product of matrices. The operator $\mathbb{G}^\perp : H_P \to H_S$ is defined by

$$\mathbb{G}^\perp = \begin{pmatrix} -\boldsymbol{D}_n \otimes \boldsymbol{I}_m \\ \boldsymbol{I}_n \otimes \boldsymbol{D}_m \end{pmatrix}.$$

It is easy to check that the restricted operator $\mathbb{G}^\perp|_{H_P^o}$ maps to H_S^o.

Finally, for discretizing the boundary condition, $\mathrm{n} \cdot u|_{\partial\Omega}$, we introduce the boundary operator

$$\mathbb{B}_\mathrm{n} : H_S \to \partial H_S := H_S \backslash H_S^o,$$

which restricts the vector field to the vectors at the grid's boundary multiplied by the outer normal vectors. The matrix form of the boundary operator is:

$$\mathbb{B}_{\mathrm{n}} = \begin{pmatrix} \boldsymbol{I}_{n-1} \otimes \boldsymbol{B}_m & \mathbf{0} \\ \mathbf{0} & \boldsymbol{B}_n \otimes \boldsymbol{I}_{m-1} \end{pmatrix},$$

where $\mathbf{0}$ are zero matrices of appropriate sizes, and

$$\boldsymbol{B}_m := \begin{pmatrix} -1 & 0 & \dots & 0 & 0 \\ 0 & 0 & \dots & 0 & 1 \end{pmatrix} \in \mathbb{R}^{2,m}.$$

It has been shown [12] that using the operators defined above, elementary properties of continuous fields in terms of div, curl, ∇, carry over to the discrete case. For example, if the curl of a vector field w is zero, $\mathbb{C}url\ w \equiv 0$, then the vector field can be expressed as the gradient of a scalar field U, $w = \mathbb{G}U$; or, if the divergence of a vector field w is a zero, $\mathbb{D}iv\ w \equiv 0$, then it should be the curl of another vector field, $w = \mathbb{G}^{\perp}U$ (recall that we only consider the 2D case in this paper).

Similarly, Green's theorem

$$\int_{\Omega} g \cdot \mathrm{div}\, u dv + \int_{\Omega} \nabla g \cdot u dv = \int_{\partial\Omega} g u_n ds \tag{2}$$

becomes in the discrete case

$$\langle g, \mathbb{D}iv\ u \rangle_{H_V} + \left\langle \overline{\mathbb{G}} g, u \right\rangle_{H_S} = \sum_{L_{\alpha,\beta} \in \partial\Omega} g_{\alpha,\beta} u_{n;\alpha,\beta}\ , \tag{3}$$

whereas Gauss' theorem

$$\int_{\Omega} \mathrm{div} u dv = \int_{\partial\Omega} u_n ds \tag{4}$$

reads in the discrete case

$$\sum_{\Omega_{\alpha,\beta} \in \Omega} \mathbb{D}iv\ u = \sum_{L_{\alpha,\beta} \in \partial\Omega} u_{n;\alpha,\beta}\ . \tag{5}$$

Using the definitions above, we rewrite this equation more concisely as

$$\mathbf{1}^{\mathrm{T}}_{\dim H_V}\, \mathbb{D}iv\ u = \mathbf{1}^{\mathrm{T}}_{\dim \partial H_S}\, \mathbb{B}_{\mathrm{n}} u\ , \tag{6}$$

where $\mathbf{1}_n$ denotes the one-vector.

Most importantly, the additional dual operators (1b) resolve the incompatibilities of domains and ranges of the primal operators (1a) when used to build *compound second order* differential operators (cf. (16) below). For example, $\mathbb{G}$ and $\mathbb{D}iv$ cannot be regarded as mutually adjoint operators, whereas $\mathbb{G},\ \overline{\mathbb{D}iv}$ and $\overline{\mathbb{G}},\ \mathbb{D}iv$ do.

2.2 Orthogonal Decomposition

We represent vector fields directly in terms of their irrotational and solenoidal components. These two components are defined by the first-order variations of velocity potentials $\psi \in H_{V+\partial V}$ and stream functions $\phi \in H_P$, and are orthogonal to each other.

Theorem 2.1 (Basic Vector Field Decomposition [13]) *For any 2D vector field $u \in H_S$, the representation of u in terms of ψ, ϕ*

$$u = \overline{\mathbb{G}}\psi + \mathbb{G}^{\perp}\phi, \quad \mathbb{B}_{\mathrm{n}}u = \mathbb{B}_{\mathrm{n}}\overline{\mathbb{G}}\psi, \tag{7}$$

where $\phi_{\partial\Omega} = 0$, is unique up to a constant of ψ.

According to (7), let:

$$u = v + w \ , \quad v = \overline{\mathbb{G}}\psi \ , \ \ w = \mathbb{G}^{\perp}\phi \ .$$

Since the operators defined in the previous section satisfy [12, 11]:

$$\mathbb{D}iv \ \mathbb{G}^{\perp} \equiv 0 \ , \qquad \overline{\mathbb{C}url} \ \overline{\mathbb{G}} \equiv 0 \ ,$$

we have

$$\mathbb{D}iv \ w = 0 \ , \qquad \overline{\mathbb{C}url} \, v = 0 \ , \tag{8}$$

and

$$\langle w, v \rangle_{H_S} = \left\langle \overline{\mathbb{G}}\psi, \mathbb{G}^{\perp}\phi \right\rangle_{H_S} = \left\langle \overline{\mathbb{C}url} \ \overline{\mathbb{G}}\psi, \phi \right\rangle_{H_P} \equiv 0 \ . \tag{9}$$

This shows:

Theorem 2.2 (Orthogonality) *The decomposition (7) is orthogonal:*

$$\left\langle \overline{\mathbb{G}}\psi, \mathbb{G}^{\perp}\phi \right\rangle_{H_S} = 0 \ , \quad \forall u \in H_S \tag{10}$$

Defining the corresponding subspaces

$$S_{ir} := \left\{ u \in H_S \,|\, u = \overline{\mathbb{G}}\psi \right\} , \tag{11}$$

$$S_{sol} := \left\{ u \in H_S \,|\, u = \mathbb{G}^{\perp}\phi, \, \phi_{\partial\Omega} = 0 \right\} , \tag{12}$$

the theorem asserts that the direct sum holds:

$$H_S = S_{ir} \oplus S_{sol} \tag{13}$$

Representation (7) is motivated by analogous decompositions of continuous vector fields [9]. However, discretizing such vector fields with standard finite differences or finite elements yields *approximate* decompositions only, which may lead to numerical instabilities in applications. In contrast, theorem 2.1 provides an *exact* orthogonal decomposition of the *finite*-dimensional space of vector fields H_S. Furthermore, as detailed below, the decomposition allows to estimate ψ and ϕ directly from a image sequence. Using variational optical

flow approaches, the estimation can be done in parallel by applying subspace correction methods. Alternatively, we may first estimate the motion field u, and then compute ψ and ϕ in a subsequent step by solving the Neumann and Dirichlet problems

$$\triangle_D \psi = \mathbb{D}iv\ u\ , \quad \mathbb{B}_{\rm n}\overline{\mathbb{G}}\psi = \mathbb{B}_{\rm n} u\ , \tag{14}$$

$$\triangle_C \phi = \overline{\mathbb{C}url}\ u\ , \quad \phi_{\partial\Omega} = 0\ , \tag{15}$$

where the discrete Laplacians are defined by

$$\triangle_D := \mathbb{D}iv\ \overline{\mathbb{G}}\ , \qquad \triangle_C := \overline{\mathbb{C}url}\ \mathbb{G}^{\perp}\ , \tag{16}$$

and the additional constraint $\mathbf{1}^{\rm T}_{{\rm dim}H_V}\ \psi = 0$ (continuous case: $\int_\Omega \psi dv = 0$) is used to eliminate the arbitrary constant in (7) and (14).

In the remainder of this paper, however, we show that directly estimating ψ, ϕ from image sequence data is feasible. Throughout we adopt the strategy to express estimation problems by direct relations between the data and unknowns. Such direct formulations allow to formulate hypotheses about unknowns in a proper way and avoid additional approximation errors through the successive application of independent techniques.

2.3 Flow Representation

Consider Gauss' theorem (5) and (6) for any vector field $u \in H_S$. We say that $\rho \in H_V$ and $\nu \in \partial H_S$ fulfill the *compatibility condition* if

$$\mathbf{1}^{\rm T}_{{\rm dim}H_V}\ \rho = \mathbf{1}^{\rm T}_{{\rm dim}\partial H_S}\ \nu \tag{17}$$

In what follows, we will make use of another flow representation, besides $u \in H_S$. To this end, consider the operator $A : H_S \rightarrow H_V \oplus H_P^o \oplus \partial H_S$ given by

$$A := \begin{pmatrix} \mathbb{D}iv \\ \overline{\mathbb{C}url} \\ \mathbb{B}_{\rm n} \end{pmatrix} \in \mathbb{R}^{{\rm dim}H_S+1, {\rm dim}H_S}\ , \tag{18}$$

where the $\overline{\mathbb{C}url}$ operator is naturally extended to the whole space H_S. The operator A has full rank ${\rm dim}H_S$. Moreover, we see by (6) that $(\rho, \omega, \nu)^{\rm T}$ is in the image of A if and only if ρ and ν fulfill the compatibility condition (17). In this case, the representation of u in terms of $(\rho, \omega, \nu)^{\rm T}$ is given by $u = A^{\dagger}(\rho, \omega, \nu)^{\rm T}$, where $A^{\dagger} = (A^{\rm T}A)^{-1}A^{\rm T}$ denotes the pseudoinverse of A.

Proposition 2.1 *There is a one–to–one correspondence between the spaces H_S and*

$$V_S := \{(\rho, \omega, \nu)^T : \mathbf{1}^T_{{\rm dim}H_V}\ \rho = \mathbf{1}^T_{{\rm dim}\partial H_S}\ \nu\}\ , \tag{19}$$

where $u \in H_S$, $\rho = \mathbb{D}iv\ u$, $\omega = \overline{\mathbb{C}url}\ u$, $\nu = \mathbb{B}_{\rm n} u$, and

$$u = A^{\dagger}(\rho, \omega, \nu)^T \tag{20}$$

Remark. In practice, we do not compute $u = A^{\dagger}(\rho, \omega, \nu)^{\mathrm{T}}$ which is ill-conditioned. Rather, we solve both the Neumann problem (14) and the Dirichlet problem (15), and insert the solutions into (7).

2.4 Extended Flow Decompositions

We take a closer look at the representation (20) by further decomposing the space V_S defined in (20). As a result, we obtain a definition of *laminar flows*, insight into the influence of boundary values, and further orthogonality relations.

The orthogonal decomposition theorem (7) shows that the two potential functions ψ, ϕ can be computed through a vector field u and its normal boundary flow $u_{\partial\Omega}$, and that the representation (13) holds. This decomposition can be rewritten in a meaningful way using the representation $(\rho, \omega, \nu)^{\mathrm{T}}$:

$$(\rho, \omega, \nu)^{\mathrm{T}} = (\rho, 0, \nu)^{\mathrm{T}} + (0, \omega, 0)^{\mathrm{T}} \tag{21}$$

Obviously, the two components, $(\rho, 0, \nu)^{\mathrm{T}}$ and $(0, \omega, 0)^{\mathrm{T}}$, are in V_S. While $(\rho, 0, \nu)^{\mathrm{T}}$ is curl-free, component $(0, \omega, 0)^{\mathrm{T}}$ is divergence-free. Let c_ρ and c_ω denote constants proportional to the mean of the divergence and the curl of u, that is

$$c_\rho \;:=\; \mathbf{1}^{\mathrm{T}}_{\dim H_V}\, \rho \;=\; \mathbf{1}^{\mathrm{T}}_{\dim H_V}\, \mathbb{D}iv\; u, \tag{22}$$

$$c_\omega \;:=\; \mathbf{1}^{\mathrm{T}}_{\dim H^o_P}\, \omega \;=\; \mathbf{1}^{\mathrm{T}}_{\dim H^o_P}\, \mathbb{C}url\; u. \tag{23}$$

Using these averaged quantities, we can further decompose the flow $u \in H_S$, represented by $(\rho, \omega, \nu)^{\mathrm{T}} \in V_S$:

$$(\rho, \omega, \nu)^{\mathrm{T}} = (c_\rho, c_\omega, \nu)^{\mathrm{T}} + (\rho^o, 0, 0)^{\mathrm{T}} + (0, \omega^o, 0)^{\mathrm{T}}, \tag{24}$$

where $\mathbf{1}^{\mathrm{T}}_{\dim H_V}\rho^o = \mathbf{1}^{\mathrm{T}}_{\dim H^o_P}\omega^o = 0$. Accordingly, we define the components

$$u = u^c + u^o_d + u^o_c$$

where $u^c := A^{\dagger}(c_\rho, c_\omega, \nu)^{\mathrm{T}}$, $u^o_d := A^{\dagger}(\rho^o, 0, 0)^{\mathrm{T}}$ and $u^o_c := A^{\dagger}(0, \omega^o, 0)^{\mathrm{T}}$. Vector u^c and $(c_\rho, c_\omega, \nu)^{\mathrm{T}}$, respectively, represent the *basic pattern* of the non-rigid flow u and its boundary distribution, while u^o_d, u^o_c and $(\rho^o, 0, 0)^{\mathrm{T}}$, $(0, \omega^o, 0)^{\mathrm{T}}$, respectively, are related to *oscillating flow patterns* that are curl-free and divergence-free. It is easy to verify that orthogonality between the components u^o_d and u^o_c is preserved

$$\langle u^o_d, u^o_c \rangle = 0,$$

while u^c and u^o_c, u^o_d are not orthogonal.

We summarize these properties, thereby extending theorem 2.1:

Proposition 2.2 (First Extended Vector Decomposition) *For any 2D vector field $u \in H_S$ and $\mathbb{B}_{\mathrm{n}} u \neq 0$, the decomposition* (24) *of u admits the representation in terms of functions ψ^c, ϕ^c, ψ^o, ϕ^o*

$$u = (\overline{\mathbb{G}}\psi^c + \mathbb{G}^{\perp}\phi^c) + \overline{\mathbb{G}}\psi^o + \mathbb{G}^{\perp}\phi^o\,, \quad \mathbb{B}_{\mathrm{n}} u = \mathbb{B}_{\mathrm{n}}\overline{\mathbb{G}}\psi^c\,, \tag{25}$$

where $\phi^c_{\partial\Omega} = \phi^o_{\partial\Omega} = 0$, $\mathbb{B}_{\mathrm{n}}\overline{\mathbb{G}}\psi^o = 0$, and $\triangle_D\psi^c \equiv$ constant, $\triangle_C\phi^c \equiv$ constant. This representation is unique up to two constants of ψ^c and ψ^o, respectively. Moreover, the orthogonality relation

$$\left\langle \overline{\mathbb{G}}\psi^o, \mathbb{G}^{\perp}\phi^o \right\rangle = 0 \tag{26}$$

holds.

While the components of the decomposition (24) and (25) are easy to interpret, a single orthogonality relation (26) only holds. To improve the latter situation, we consider the alternative decomposition

$$(\rho, \omega, \nu)^{\mathrm{T}} = (c_\rho, 0, \nu)^{\mathrm{T}} + (\rho^o, 0, 0)^{\mathrm{T}} + (0, \omega, 0)^{\mathrm{T}} \,. \tag{27}$$

The corresponding components of $u \in H_S$ are denoted as

$$u = u^c_d + u^o_d + u_c$$

where $u^c_d := A^{\dagger}(c_\rho, 0, \nu)^{\mathrm{T}}$, $u^o_d := A^{\dagger}(\rho^o, 0, 0)^{\mathrm{T}}$ and $u_c := A^{\dagger}(0, \omega, 0)^{\mathrm{T}}$. As will be shown below, this decomposition provides the basis for representing any vector field, under additional conditions to be specified, by three mutually orthogonal components. We first summarize the properties of (27):

Proposition 2.3 (Second Extended Vector Decomposition) *For any 2D vector field $u \in H_S$ and $\mathbb{B}_{\mathrm{n}}u \neq 0$, the decomposition* (27) *of u admits the representation in terms of functions ψ^c, ψ^o, ϕ*

$$u = \overline{\mathbb{G}}\psi^c + \overline{\mathbb{G}}\psi^o + \mathbb{G}^{\perp}\phi \,, \quad \mathbb{B}_{\mathrm{n}}u = \mathbb{B}_{\mathrm{n}}\overline{\mathbb{G}}\psi^c \,, \tag{28}$$

where $\phi_{\partial\Omega} = 0$, $\mathbb{B}_{\mathrm{n}}\overline{\mathbb{G}}\psi^o = 0$, and $\triangle_D\psi^c \equiv$ constant. This representation is unique up to two constants of ψ^c and ψ^o, respectively. Moreover, the orthogonality relations

$$\left\langle \overline{\mathbb{G}}\psi^o, \mathbb{G}^{\perp}\phi \right\rangle = 0 \,, \qquad \left\langle \overline{\mathbb{G}}\psi^c, \mathbb{G}^{\perp}\phi \right\rangle = 0$$

hold.

It remains to work out conditions under which the flow components $\overline{\mathbb{G}}\psi^c$ and $\overline{\mathbb{G}}\psi^o$ are orthogonal, too. By Green's theorem (3), we have

$$\left\langle \overline{\mathbb{G}}\psi^o, \overline{\mathbb{G}}\psi^c \right\rangle = - \left\langle \psi^o, \triangle_D\psi^c \right\rangle + \left\langle \psi^o, \nu \right\rangle_{\partial\Omega}$$

Taking into account the compatibility condition (17), $\mathbf{1}^{\mathrm{T}}_{\dim H_V}\triangle_D\psi^c = \mathbf{1}^{\mathrm{T}}_{\dim\partial H_S}\nu$, we observe that the right hand side is invariant with respect to an arbitrary additive constant C of ψ^o:

$$\begin{aligned} - \left\langle \psi^o + C, \triangle_D\psi^c \right\rangle + \left\langle \psi^o + C, \nu \right\rangle_{\partial\Omega} &= - \left\langle \psi^o, \triangle_D\psi^c \right\rangle + \left\langle \psi^o, \nu \right\rangle_{\partial\Omega} \\ &\quad + C(-\mathbf{1}^{\mathrm{T}}_{\dim H_V}\triangle_D\psi^c + \mathbf{1}^{\mathrm{T}}_{\dim\partial H_S}\nu) \\ &= - \left\langle \psi^o, \triangle_D\psi^c \right\rangle + \left\langle \psi^o, \nu \right\rangle_{\partial\Omega} . \end{aligned}$$

Hence, fixing this constant by setting $\langle \psi^o, \nu \rangle = 0$, we obtain

$$- \langle \psi^o, \triangle_D \psi^c \rangle + \langle \psi^o, \nu \rangle_{\partial\Omega} = -c_\rho \mathbf{1}^{\mathrm{T}}_{\dim H_V} \psi^o \ ,$$

because $\triangle_D \psi^c$ is constant by proposition 2.3. It follows that $\left\langle \overline{\mathbb{G}} \psi^o, \overline{\mathbb{G}} \psi^c \right\rangle = 0$ if $c_\rho = 0$. This means that the total divergence of flow u is zero, and that the flow entering and leaving the domain Ω is balanced

$$\mathbf{1}^{\mathrm{T}}_{\dim H_V} \mathbb{D}iv \ u = \mathbf{1}^{\mathrm{T}}_{\dim \partial H_S} \nu = 0.$$

Proposition 2.4 (Extended Orthogonal Vector Decomposition) *Suppose $u \in H_S$ is a 2D vector field with $\mathbb{B}_{\mathrm{n}} u \neq 0$, and that the balanced boundary flow condition*

$$\mathbf{1}^{T}_{\dim \partial H_S} \mathbb{B}_{\mathrm{n}} u = 0$$

holds. Then u can be represented in terms of functions ψ^c, ψ^o, ϕ

$$u = \overline{\mathbb{G}} \psi^c + \overline{\mathbb{G}} \psi^o + \mathbb{G}^{\perp} \phi \, , \quad \mathbb{B}_{\mathrm{n}} u = \mathbb{B}_{\mathrm{n}} \overline{\mathbb{G}} \psi^c \ , \tag{29}$$

where $\phi_{\partial\Omega} = 0$, $\mathbb{B}_{\mathrm{n}} \overline{\mathbb{G}} \psi^o = 0$, and $\triangle_D \psi^c \equiv 0$. This representation is unique up to two constants of ψ^c and ψ^o, respectively, and all three components $\overline{\mathbb{G}} \psi^c$, $\overline{\mathbb{G}} \psi^o$ and $\mathbb{G}^{\perp} \phi$, are mutually orthogonal.

Note that the basic part $\overline{\mathbb{G}} \psi^c$ turns out to be the *laminar flow*, i.e. it is both divergence and curl free.

As a consequence of proposition 2.4, we can refine the decomposition (13) of the vector field space H_S. To this end, we define further subspaces in addition to (11) and (12):

$H_{S,\bar{o}} \subset H_S$	subspace of vector fields with $\mathbf{1}^{\mathrm{T}}_{\dim \partial H_S} \mathbb{B}_{\mathrm{n}} u = 0$
$S_{ir,o} \subset S_{ir}$	subspace of irrotational vector fields with zero boundary flow
$S_{ir,C} \subset S_{ir}$	subspace of irrotational vector fields with constant divergence
$S_{div,0}$	subspace of vector fields with vanishing divergence
S_{lam}	subspace of vector fields with vanishing divergence and curl

Based on these definitions, we summarize consequences of proposition 2.4:

Corollary 2.1 *2D vector fields $u \in H_S$ admit the following decompositions:*

$$H_S = (S_{ir,C} + S_{ir,o}) \oplus S_{sol} \tag{30}$$

$$H_{S,\bar{o}} = S_{ir,C} \oplus S_{ir,o} \oplus S_{sol} \tag{31}$$

$$S_{div,0} = S_{lam} \oplus S_{sol} \tag{32}$$

3 Variational Approaches

In this section, we present and discuss various variants of the following variational approach to optical flow estimation:

$$\min_{u \in H_S} F(u) \ , \quad F(u) := \| I_1(x+u) - I_2(x) \|^2_{H_V} + L(u) \tag{33}$$

Here, $I_1, I_2 \in H_V$ are subsequent images of a given sequence, and $L(u)$ is a regularizing term to be specified below, which makes the variational problem well-posed.

We point out that the data term – the first term in (33) – could be made robust against outliers by using some robust estimators or the L^1-norm [4]. In this paper, however, we focus on higher-order regularization in connection with the representation (7).

3.1 Data Term

In order to alleviate the local minima problem and to capture large motions, we apply the standard procedure of minimizing $F(u)$ using a sequence of linearizations of the data term

$$F^l(u^l) := \left\| \overline{\mathbb{G}} I_1^l \cdot u^l + \partial_t I^l \right\|_{H_V}^2 + L(u^l) \ , \tag{34}$$

where $\{I_1^l, I_2^l\}_{l=0,1,\ldots,m}$ denote linear scale-space representations of a given image pair, and $\partial_t I^l = I_1^l(x) - I_2^l(x - u^{l+1}(x))$.

In this connection, the prolongation operator transferring various quantities to the next finer grid deserves special attention, in order to preserve properties based on the decomposition (7). A corresponding constrained interpolation scheme will be detailed in section 5.3.

3.2 Div-Curl Regularization

We wish to apply the following second-order regularizer (cf. the discussion of related work in section 1):

$$\int_\Omega \lambda_1 |\nabla \mathrm{div}\, u|^2 + \lambda_2 |\nabla \mathrm{curl}\, u|^2 dx = \int_\Omega \lambda_1 |\nabla \triangle\, \psi|^2 + \lambda_2 |\nabla \triangle\, \phi|^2 dx \tag{35}$$

where λ_1 and λ_2 are two positive constants. This term measures the variation of the basic flow components divergence and curl, but *does not penalize* the components themselves. However, both standard finite differences or finite elements discretization lead to finite-dimensional representations which do not satisfy (7) and (10). As a result, penalizing one component may affect the other component too. Therefore, we adopt the framework of section 2.2 which leads to the following discretization of (35):

$$\begin{aligned} L(u) := L_{div}(u) + L_{curl}(u) :=& \lambda_1 \left\| \overline{\mathbb{G}} \mathbb{D}iv\, u \right\|_{H_S}^2 + \lambda_2 \left\| \mathbb{G} \overline{\mathbb{C}url}\, u \right\|_{H_E}^2 & (36) \\ =& \lambda_1 \left\| \overline{\mathbb{G}} \triangle_D \psi \right\|_{H_S}^2 + \lambda_2 \left\| \mathbb{G} \triangle_C \phi \right\|_{H_E}^2 & (37) \end{aligned}$$

3.3 Potential Based Non-rigid Flow Estimation

For the general non-rigid flow estimation, we consider the functional

$$\min_{u \in H_S} F(u) \ , \quad F(u) := \|I_1(x+u) - I_2(x)\|_{H_V}^2 + L_{div}(u) + L_{curl}(u) \tag{38}$$

Inserting the decomposition (7) and (37), we obtain the minimization problem

$$\min_{\psi,\phi} F(\psi,\phi)\ , \quad F(\psi,\phi) = \left\| I_1(x + \overline{\mathbb{G}}\psi + \mathbb{G}^{\perp}\phi) - I_2(x) \right\|_{H_V}^2 + \lambda_1 \left\| \overline{\mathbb{G}} \triangle_D \psi \right\|_{H_S}^2 + \lambda_2 \left\| \mathbb{G} \triangle_C \phi \right\|_{H_E}^2 \tag{39}$$

subject to the linear constraints

$$\mathbf{1}_{\dim \partial H_V}^{\mathrm{T}} \psi = 0\ , \quad \phi_{\partial\Omega} = 0 \tag{40}$$

Note that the first constraint fixes the free constant mentioned in theorem 2.1. Furthermore, the vector fields in (39) are elements of orthogonal subspaces (13), and thus may be determined in parallel by subspace correction methods.

3.4 Estimation of Solenoidal Flows

An important special case, particularly in applications of experimental fluid dynamics, concerns the estimation of divergence-free flows. In this case the decomposition (29) reduces to (cf. (32)):

$$u = \overline{\mathbb{G}}\psi^c + \mathbb{G}^{\perp}\phi := u_d^c + u_c \tag{41}$$

with the laminar flow $u_d^c = \overline{\mathbb{G}}\psi^c$ which only depends on the boundary flow $\mathbb{B}_{\mathrm{n}} u$:

$$\triangle_D \psi^c = 0\ , \quad \mathbb{B}_{\mathrm{n}} \overline{\mathbb{G}} \psi^c = \mathbb{B}_{\mathrm{n}} u. \tag{42}$$

In order to estimate solenoidal flows, we consider instead of (39) the functional

$$\min_{u \in S_{div0}} F_{sol}(u)\ , \quad F_{sol}(u) := \| I_1(x+u) - I_2(x) \|_{H_V}^2 + L_{curl}(u) \tag{43}$$

Inserting the decomposition (41), we obtain the minimization problem:

$$\min_{\psi^c,\phi} F_{sol}(\psi^c,\phi)\ , \quad F_{sol}(\psi^c,\phi) = \left\| I_1(x + \overline{\mathbb{G}}\psi^c + \mathbb{G}^{\perp}\phi) - I_2(x) \right\|_{H_V}^2 + \lambda \left\| \mathbb{G} \triangle_C \phi \right\|_{H_E}^2 \tag{44}$$

subject to the constraints:

$$\triangle_D \psi^c = 0\ , \quad \mathbf{1}_{\dim \partial H_V}^{\mathrm{T}} \psi^c = 0\ , \quad \phi_{\partial\Omega} = 0 \tag{45}$$

Note that the vector fields of (44) are elements of orthogonal subspaces (32), and thus may be determined in parallel by subspace correction methods.

3.5 Third-order Derivative Regularizers

In both variational approaches (39) and (44) third-order regularizers appear in the energy functional. A common method to reduce the order of the regularizer is to use auxiliary variables $\xi_1 = \triangle_D \psi$ and $\xi_2 = \triangle_C \phi$ resulting in first-order terms:

$$L_{div} = \lambda_1 \left\| \overline{\mathbb{G}} \xi_1 \right\|_{H_S}^2\ ,\ L_{curl} = \lambda_2 \left\| \mathbb{G} \xi_2 \right\|_{H_E}^2\ , \quad \text{with} \quad \xi_1 = \triangle_D \psi\ ,\ \xi_2 = \triangle_C \phi \tag{46}$$

In principle, this has the advantage to decrease the order of the regularizers. On the other hand, imposing the equations $\xi_1 = \triangle_D \psi\,,\ \xi_2 = \triangle_C \phi$ as hard constraints requires a careful analysis of the underlying continuous setting in order to avoid a mismatch of spaces and boundary constraints. Therefore, such equations are mostly applied in a least-squares sense in the literature, which introduces additional errors. In contrast, through the mimetic finite-difference method it is possible to directly obtain problem discretizations which are both accurate and stable.

4 Well-posedness and Stability

In this section, we analyse well-posedness of the variational approaches discussed in section 3. To this end, we state the conditions under which the respective functionals are strictly convex. This will be done for a single level l in (34), and in terms of vector fields u due to the unique representations stated in theorem 2.1 and proposition 2.4. These representations also allow us to point out in section 4.3 a potential source of instability in connection with the higher-order regularizer from section 3.2. This result appears to be new in the literature. Furthermore, our experimental results showed that removing this instability as developed below, is numerically significant.

In order to compactly state the various conditions for well-posedness, we complement the list of subspaces defined at the end of section 2.4. To this end, we define the linear operator

$$G := (\overline{\mathbb{G}} I_1 \cdot\ )\ ,$$

and use the notation $N(A)$ for the null-space of a linear operator A:

$S_{sol,C} \subset S_{sol}$	subspace of solenoidal vector fields with constant curl
$H_{S,C} \subset H_S$	subspace of vector fields $H_{S,C} := S_{ir,C} + S_{sol,C} = N(\overline{\mathbb{G}}\mathbb{D}iv\ ) \cap N(\mathbb{G}\overline{\mathbb{C}url}\ )$
$S_{G0} \subset H_S$	subspace of vector fields $S_{G0} = \{u \mid Gu = 0\}$

4.1 Well-posedness of General Flows

The variational approach (33) for estimating general flows amounts to the unconstrained convex minimization problem:

$$\min_{u \in H_S} F(u)\ , \quad F(u) = \|Gu + \partial_t I\|^2_{H_V} + \lambda_1 \left\|\overline{\mathbb{G}}\mathbb{D}iv\ u\right\|^2_{H_S} + \lambda_2 \left\|\mathbb{G}\overline{\mathbb{C}url}\ u\right\|^2_{H_E} \tag{47}$$

As a consequence, the following is immediate:

Proposition 4.1 *Problem* (33) *is well-posed if and only if*

$$S_{G0} \cap H_{S,C} = \{0\}$$

As the subspace $H_{S,C}$ is fixed with the problem dimension, this condition requires a sufficiently high spatial variation of the grayvalue image I to obtain well-posedness. A counterexample is given by any image I with $\triangle_D I \equiv \mathbb{C}url\ \overline{\mathbb{G}}^{\perp} I = C$, because for the vector field $\overline{\mathbb{G}}^{\perp} I \in H_E$ the inner product with $\overline{\mathbb{G}} I \cdot \overline{\mathbb{G}}^{\perp} I$, computed by summing up the corresponding local expressions over all cells (see fig. 1), vanishes.

4.2 Well-posedness on Solenoidal Flows

The variational approach (43) for estimating divergence-free flows amounts to a convex quadratic minimization problem with linear equality constraints. Expressing the restriction $u \in S_{lam} \oplus S_{sol}$ through the constraint $\mathbb{D}iv\ u = 0$, we reformulate (43):

$$\min_{u \in H_S} F_{sol}(u)\ , \quad F_{sol}(u) = \|Gu + \partial_t I\|^2_{H_V} + \lambda \left\|\mathbb{G}\overline{\mathbb{C}url}\ u\right\|^2_{H_E}\ , \ \text{s.t.}\ \mathbb{D}iv\ u = 0 \tag{48}$$

As a consequence, the condition for well-posedness reads:

Proposition 4.2 *Problems* (43) *and* (48) *are well-posed if and only if*

$$S_{G0} \cap (S_{lam} \oplus S_{sol,C}) = \{0\}$$

Note that problem (48) apparently gives rise to three relevant null-spaces, S_g, $S_{sol,C}$, and $S_{lam} \oplus S_{sol}$. However, because $S_{sol,C} \subset S_{sol}$, we have

$$S_{sol,C} \cap (S_{lam} \oplus S_{sol}) = S_{lam} \oplus S_{sol,C}\ .$$

4.3 Stability

It is well-known that existence of a unique solution, as established in the previous section, does not say much about *numerical* stability. Indeed, inspection of the second-order regularizer (35) reveals a particular sensivity of u with respect to the image data and suggests using a corresponding regularizer.

To motivate this additional term, we rewrite the estimation functional using the representation $(\rho, \omega, u_{\partial\Omega})^{\mathrm{T}}$ (cf. prop. 2.1):

$$\min_{\rho,\omega,u_{\partial\Omega}} F(u)\ , \quad F(u) = \left\|GA^{\dagger}(\rho, \omega, u_{\partial\Omega})^{\mathrm{T}} + \partial_t I\right\|^2 + \lambda_1 \|\nabla\rho\|^2 + \lambda_2 \|\nabla\omega\|^2 \tag{49}$$

We consider the extended decomposition due to theorem 2.3 and (30). Considering (27), the variance of divergence and curl field related to the two components $(\rho^o, 0, 0)^{\mathrm{T}}$ and $(0, \omega, 0)^{\mathrm{T}}$ can be penalized and constrained by the respective regularizers. However, for the last part $(c_\rho, 0, \nu)^{\mathrm{T}}$ which is curl-free and has constant divergence, both regularization terms are not effective.

The discussion in section (2.4) showed that this part only depends on the normal flow at the boundary $u_{\partial\Omega}$. In fact, $(c_\rho, 0, \nu)^{\mathrm{T}}$ is only weakly constrained by the data term, that is

the gradient field of image data I at the boundary whose estimate is noisy and unreliable. Therefore, in practice, it turned out to be useful to reduce this sensivity of u by including a regularizer which additionally constrains the boundary values:

$$\int_{\partial\Omega} (\partial_n u)^2 \, dl \tag{50}$$

This constraint term favors continuity of vector field $u(\Omega)$ between the boundary and the interior domain. By virtue of the orthogonal decomposition, it can be directly expressed in terms of ψ.

5 Algorithms and Implementation

In this paper, we apply the space decomposition method to restore the two potential fields $\phi(\Omega)$ and $\psi(\Omega)$ directly. This method provides a general framework for analysing domain decomposition and multigrid methods [23] [24]. The essence is to decompose the solution space into a sum of subspaces and then solve the original optimization problem sequentially or in parallel in each subspace. Extensions to some convex optimization problems were presented in [20], and convergence rates are analyzed in [18, 21, 19].

We describe the space decomposition method and its application to our approach in sections 5.1 and 5.2. Subsequently, we detail in sections 5.3 and 5.4 a multi-level representation of flow fields adapted to the orthogonal decomposition.

5.1 Iterative Subspace Corrections

Suppose that for a general convex optimization problem

$$\min_{u \in V} F(u) \ , \tag{51}$$

the solution function space V can be decomposed into a sum of subspaces

$$V = V_1 + V_2 + \ldots + V_m \ . \tag{52}$$

For any $u \in V$, there exist $u_i \in V_i$, such that $u = \sum_{i=1}^{m} u_i$. Conversely, if $u_i \in V_i$, then $\sum_{i=1}^{m} u_i \in V$. Note that in general the sum is not the direct sum, and the decomposition of u is not unique.

There are two versions of iterative algorithms, the Parallel Subspace Corrections (PSC) and the Successive Subspace Corrections (SSC). In each step, PSC and SSC compute the next iterate in V through searching each subspaces V_i, $i = 1, \ldots, m$, in parallel or sequentially, respectively. With suitable assumptions about the objective function $F(u)$ and the space decomposition scheme, both algorithms converge. As we do not focus on parallel implementations in this work, we adopted SSC which, in this case, converges faster.

Algorithm 5.1 (Successive Subspace Corrections) .

- *Step 1. Choose $u_i^0 \in V_i$.*
- *Step 2. For the n-th iteration, compute $\hat{u}_i^{n+1} \in V_i$ sequentially for $i = 1, \ldots, m$, by minimization:*

$$F\big(\sum_{1\le k<i} u_k^{n+1} + \hat{u}_i^{n+1} + \sum_{i<k\le m} u_k^n\big) \le F\big(\sum_{1\le k<i} u_k^{n+1} + v_i + \sum_{i<k\le m} u_k^n\big), \quad \forall v_i \in V_i. \tag{53}$$

Choose $u_i^{n+1} \in V_i\,,\ i = 1, \ldots, m$, such that

$$\left\|u_i^{n+1} - \hat{u}_i^{n+1}\right\|_V \le \epsilon_0 \left\|u_i^n - \hat{u}_i^{n+1}\right\|_V \ , \quad 0 \le \epsilon_0 \le 1 \ . \tag{54}$$

- *Step 3. Go to the next iteration.*

In practice, we choose $u_i^{n+1} = (1-\epsilon_0)\hat{u}_i^{n+1} + \epsilon_0 u_i^n$, with $\epsilon_0 \in [0.5, 0.75]$.

5.2 Application to Flow Estimation

Based on algorithm 5.1, the estimation of general flows amounts to solving the two subproblems

$$\min_{\psi} \widetilde{F}(\psi, \bar{\phi}) \ , \quad \widetilde{F}(\psi, \bar{\phi}) = \left\|I(x + \overline{\mathbb{G}}\psi + \mathbb{G}^{\perp}\bar{\phi}) - I(x)\right\|_{H_V}^2 + \lambda_1 \left\|\overline{\mathbb{G}}\triangle_D \psi\right\|_{H_S}^2 \ , \tag{55}$$

$$\min_{\phi} \widetilde{F}(\bar{\psi}, \phi) \ , \quad \widetilde{F}(\bar{\psi}, \phi) = \left\|I(x + \overline{\mathbb{G}}\bar{\psi} + \mathbb{G}^{\perp}\phi) - I(x)\right\|_{H_V}^2 + \lambda_2 \left\|\mathbb{G}\triangle_C \phi\right\|_{H_E}^2 \ , \tag{56}$$

where $\bar{\psi}$ and $\bar{\phi}$ are fixed variables at each iteration. Each subproblem is an unconstained convex quadratic problem to which the preconditioned conjugate gradient iteration [16] was applied.

Concerning estimation of divergence-free flows, approach (44) together with (45) requires as part of algorithm 5.1 to solve a linearly constrained quadratic problem in the subspace of laminar flows. To this end, the Augmented Lagrangian Method is applied. For details, we refer to [3]. The corresponding augmented Lagrangian function for the $\psi-$subproblem reads:

$$L_{\bar{\phi}}(\psi^c, r) = \left\|I(x + \overline{\mathbb{G}}\psi^c + \mathbb{G}^{\perp}\bar{\phi}) - I(x)\right\|^2 + \langle r, \triangle_D \psi^c\rangle + \frac{c}{2}\left\|\triangle_D \psi^c\right\|_{H_V}^2 \ , \tag{57}$$

with $\bar{\phi}$ being fixed at each iteration step. Direct incorporation into the augmented Langrangian iteration of the remaining linear equality $\sum_{H_V} \psi = 0$ in (45) would destroy the sparsity of the matrix of the penalty term and, in turn, the efficiency of the sparse solver. Instead, we simply remove the average from iterates $(\psi^c)^n$ as a simple post-processing step.

In practice, the augmented Lagrangian iteration converged in less than 10 iterations.

5.3 Multi-level Implementation

Related to section 3.1, we detail in this and in the following section the multi-level handling of flow fields in terms of potential functions ψ, ϕ.

According to section 2.2, discrete fields of divergence $(\mathbb{D}iv\ u)^l\ ,\ l = 1, \ldots, m$, are elements of the space H_V, and fields $(\overline{\mathbb{C}url}\, u)^l\ ,\ l = 1, \ldots, m$, are in H_P^o.

As described in [14, 15], two image pyramids $\{I_i^l\}_{l=1,\ldots,m}\ ,\ i = 1, 2$, are constructed. $l = 0$ denotes the original image, and $l = m$ denotes the coarsest level. At level l, given potential fields $\tilde{\psi}^l$, $\tilde{\phi}^l$ and the velocity field $\tilde{u}^l = \overline{\mathbb{G}}\tilde{\psi}^l + \mathbb{G}^\perp\tilde{\phi}^l$, image I_2^l is warped to $\tilde{I}_2^l = I_2^l(x - \tilde{u}^l)$. The image flow between the two images $\tilde{I}_1^l$ and I_2^l is assumed to be small enough to allow for accurate linearization:

$$\partial_t I^l = I_1^l - \tilde{I}_2^l \tag{58}$$

$$\Delta_u^l = \overline{\mathbb{G}} I_1^l \cdot (u^l - \tilde{u}^l) \tag{59}$$

$$\Delta_{\psi,\phi}^l = \overline{\mathbb{G}} I_1^l \cdot (\overline{\mathbb{G}}(\psi^l - \tilde{\psi}^l) + \mathbb{G}^\perp(\phi^l - \tilde{\phi}^l)). \tag{60}$$

The residual motion field u^l, in terms of $\overline{\mathbb{G}}\psi^l + \mathbb{G}^\perp\phi^l$, is estimated by solving the problem

$$\min_{\psi^l,\phi^l} F(\psi^l, \phi^l)\ , \quad F(\psi^l, \phi^l) = \left\|\Delta_{\psi,\phi}^l + \partial_t I^l\right\|_{H_V}^2 + \lambda_1 \left\|\overline{\mathbb{G}}\triangle_D \psi^l\right\|_{H_S}^2 + \lambda_2 \left\|\mathbb{G}\triangle_C \phi^l\right\|_{H_E}^2 \tag{61}$$

The minimizer ψ^l, ϕ^l and u^l are postprocessed to yield the initialization $\tilde{\psi}^{l-1}$, $\tilde{\phi}^{l-1}$ and $\tilde{u}^{l-1}$ of the next finer level $l-1$, as discussed in the following section. The whole process is started at the coarsest level m with $\tilde{\psi}^m = 0$, $\tilde{\phi}^m = 0$ and $\tilde{u}^m = 0$.

5.4 Constrained Prolongation

It is important to preserve the subspace properties during grid transfer. Corresponding divergence- and curl-preserving interpolation schemes for vector fields are suggested in [22, 5]. In this work, however, we transfer potential fields ψ^l and ϕ^l to the next level $l-1$, rather than u^l.

This is done by bilinearly interpolating the divergence ρ^l, the curl ω^l, and the boundary values of ψ^l, to obtain $\tilde{\rho}^{l-1}, \tilde{\omega}^{l-1}$ and $\tilde{\psi}_{\partial\Omega}^{l-1}$ (cf. the notation of the previous section). Then $\tilde{\psi}^{l-1}$ is computed as solution to

$$\triangle_D \psi = \tilde{\rho}^{l-1}\ , \quad \text{s.t.} \quad \psi_{\partial\Omega} = \tilde{\psi}_{\partial\Omega}^{l-1}\ . \tag{62}$$

Analogously, we compute $\tilde{\phi}^{l-1}$ as solution to

$$\triangle_C \phi = \tilde{\omega}^{l-1}\ , \quad \text{s.t.} \quad \phi_{\partial\Omega} = 0\ . \tag{63}$$

The corresponding veloctiy field $\tilde{u}^{l-1}$ at the next finer level $l-1$ is

$$\tilde{u}^{l-1} = \overline{\mathbb{G}}\tilde{\psi}^{l-1} + \mathbb{G}^\perp\tilde{\phi}^{l-1}\ . \tag{64}$$

6 Experiments

In this section, we validate our approach with few numerical experiments. A more thorough evaluation from the viewpoint of experimental fluid dynamics is beyond the scope of this work and will be reported elsewhere.

6.1 Error Measures

In pactice, evaluating non-rigid flows by computing the average angular and norm error, respectively, induced by the inner product of the space $(L^2(\Omega))^2 = L^2(\Omega) \times L^2(\Omega)$ [2], appeared to us too insensitive to the important flow structures. Therefore, we suggest error measures that also take into account divergence and curl of flow structures:

$$e_{norm} := \frac{\langle w, w \rangle_{DC}}{N} \;, \quad e_{ang} := \arccos \frac{\langle u, v \rangle_{DC} + 1}{\sqrt{\langle u, u \rangle_{DC} + 1}\sqrt{\langle v, v \rangle_{DC} + 1}} \;, \tag{65}$$

where we adopt the average angular and norm error measures but use the inner products of the space $H(\mathrm{div}; \Omega) \cap H(\mathrm{curl}; \Omega)$ (see, e.g., [9]):

$$\langle u, v \rangle_{DC} := \langle u, v \rangle_{H_S} + \langle \mathbb{D}iv\; u, \mathbb{D}iv\; v \rangle_{H_V} + \left\langle \overline{\mathbb{C}url}\; u, \overline{\mathbb{C}url}\; v \right\rangle_{H_P} . \tag{66}$$

6.2 Experiment Results

6.2.1 Ground truth experiments

Figure 2 shows a synthetic image which was warped by the indicated flow. The corresponding errors for the approach (44), $e_{norm} = 6.1e-3\,,\ e_{ang} = 6.51°$, are smaller than the approach with Horn-Schunck regularization: $e_{norm} = 2.95e-2\,,\ e_{ang} = 13.52°$. Note, that these error measures include flow derivatives as opposed to common measures used in the literature. It can be clearly observed that the divergence distribution of the flow recovered by our method (figure 2, right) is close to zero (below 10^{-12}), in comparison to the Horn-Schunck method (middle figure 2).

6.2.2 Estimating Solenoidal Flows

Figure 3 shows the result of estimating the solenoidal flow for a real image sequence based on the multi-level framework. The comparison with first-order regularization (Horn-Schunck approach) in Figure 4 cleary reveals the superiority of our approach regarding the reconstruction of vortex structures. Furthermore, the (in this case) physically plausible constraint of vanishing divergence is satisfied quite accurately.

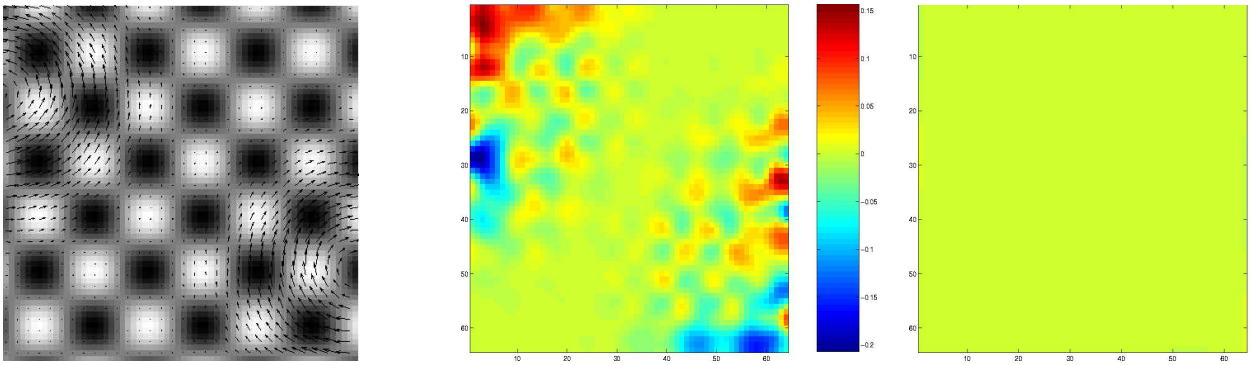

Figure 2: **Left:** Synthetic image and solenoidal velocity field. **Middle:** Divergence error using Horn-Schunck regularization. **Right:** Divergence error using our approach.

6.2.3 Estimating General Non-Rigid Flows

Figures 5 and 6 show general non-rigid flow estimated for two different real image sequences. As in the solenoidal case, the potential functions provide a useful representation of qualitative properties of the flow. These experiments have been performed on images of the infra-red channel of the meteosat satellite. They show respectively exploding convective cells (fig. 5) and a trough of low pressure (fig. 6, left) and a convective system (fig. 6, right).

6.2.4 Application to Particle Image Velocimetry (PIV)

Figure 7 shows the result of our approach applied to the PIV image sequence from a flow around two cylinders. The divergence field and curl field inside the area of two cylinders are close to zero since the motion field is zero. Note that the two potential fields $\psi(\Omega)$ and $\phi(\Omega)$ are not zero in these domains, but rather the sum of $\nabla\psi$ and $\nabla^{\perp}\phi$ is.

Figure 8 shows the results computed from a PIV image pairs of a liquid freezing experiment, recorded by Tomasz A. Kowalewski (`http://www.ippt.gov.pl/~tkowale/`).

7 Conclusion and Future Works

We introduced mathematically sound discrete representations of vector fields for estimating highly non-rigid flows from image sequences. The estimation is directly done in terms of component functions that decompose flows into orthogonal subspaces and reveal quantitative information of physical relevance.

Our further work will focus on the use of multigrid iterations for accelerating the subproblem solvers, on evaluations and applications from the viewpoint of experimental fluid dynamics (cf., e.g. [15, 6], and on the extension to 3D image sequences.

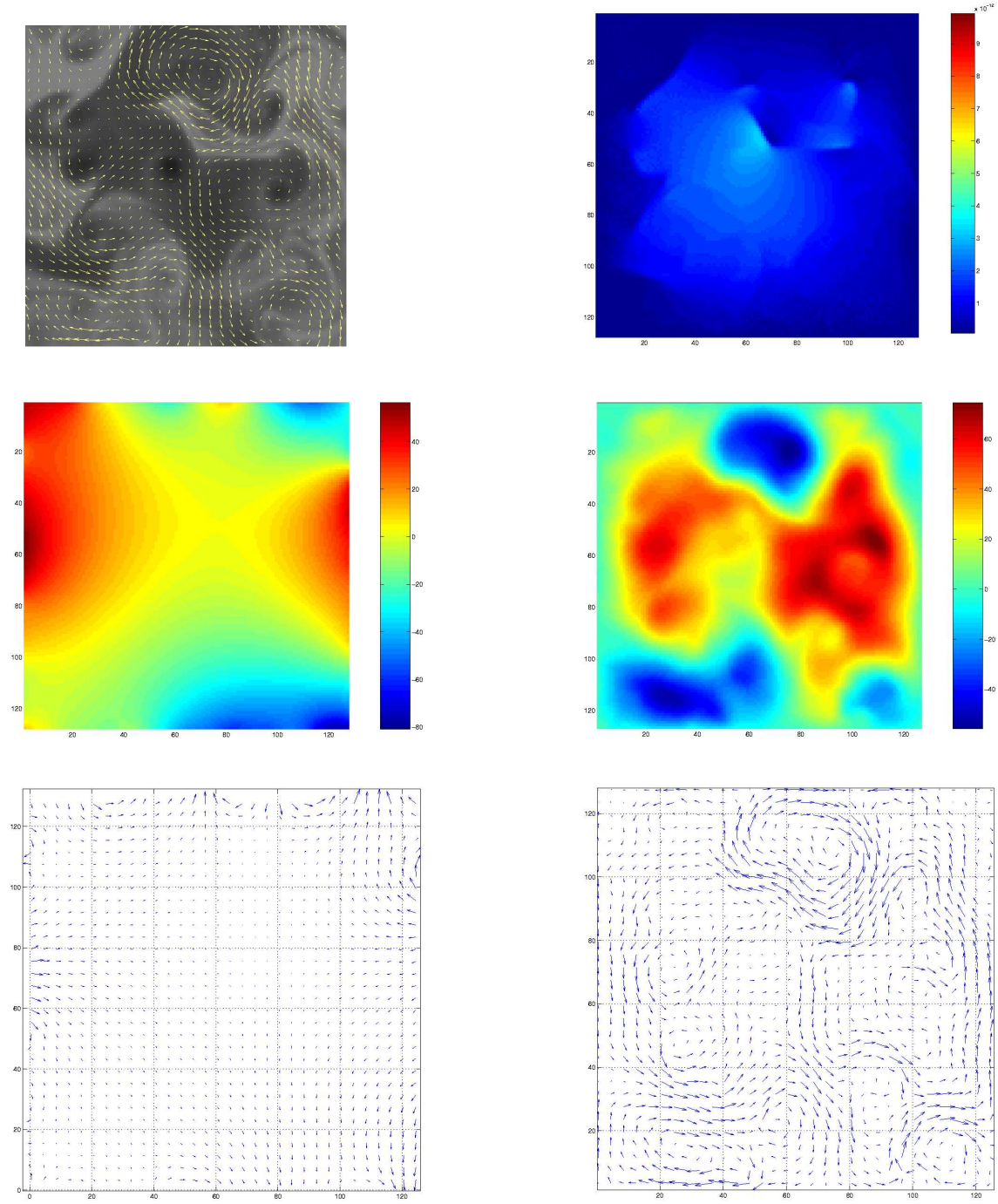

Figure 3: **Top Left** The first image $I_1$with the restored solenoidal flow. **Top Right** The divergence field of the flow which is less than $3 * 10^{-12}$. **Middle Left** The potential field $\psi_l(\Omega)$ related to the laminar flow. **Middle Right** The potential field $\phi(\Omega)$. **Bottom Left** The first component of flow: the laminar flow u_{lam}. **Bottom Right** The second component of flow related to potential $\phi(\Omega)$. The comparison with standard regularization is depicted in Figure 4.

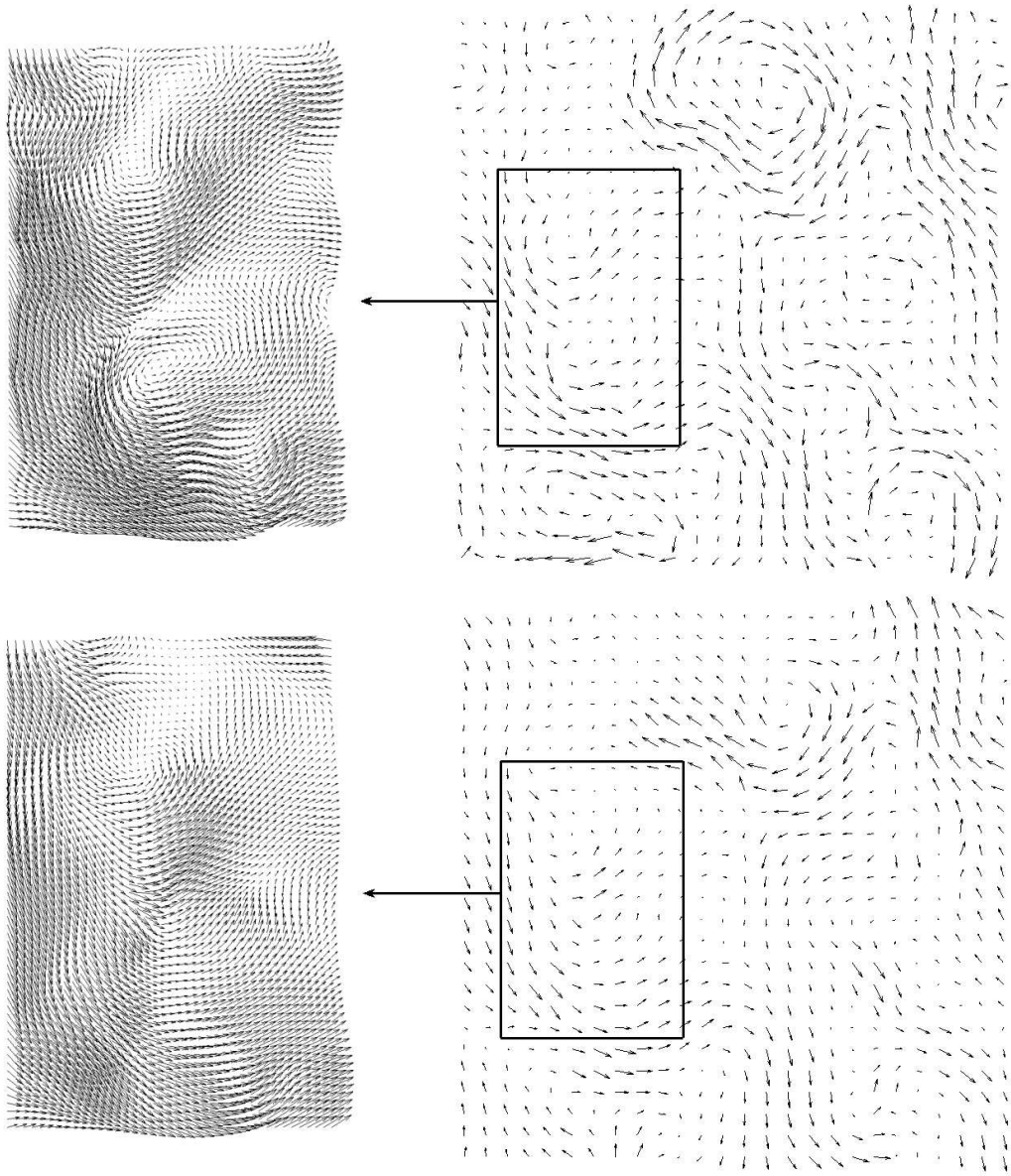

Figure 4: **Top** The restored solenoidal flow $u(\Omega)$. **Bottom** The restored flow $u_{hs}(\Omega)$ using the Horn-Schunck regularization. This results clearly show that vortex structures are better recovered by our approach. Furthermore, the magnitude of the divergence is below 10^{-11} throughout the image plane.

Acknowledgement

This work was supported by the European project FLUID.

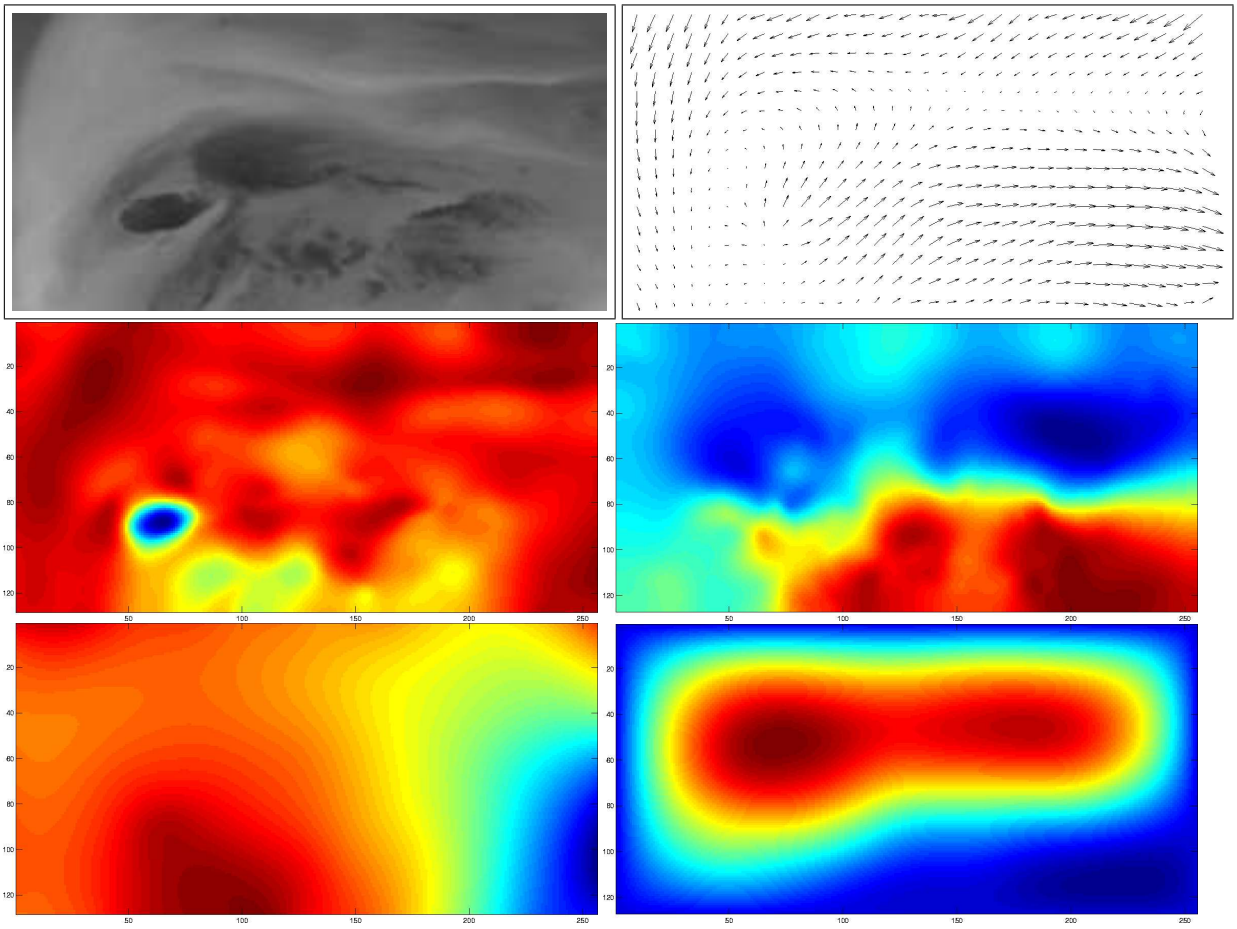

Figure 5: **Top** Image I with the restored flow field u. **Middle Left** The divergence field of u. **Middle Right** The curl field of u. **Bottom Left** The potential field $\psi(\Omega)$. **Bottom Right** The potential field $\phi(\Omega)$. The divergence field, for example, which clearly detects a "source" (blue blob), illustrates the quality and usefulness of the results.

References

[1] L. Amodei and M. N. Benbourhim. A vector spline approximation. *J. Approx. Theory*, 67(1):51–79, 1991.

[2] J. L. Barron, D. J. Fleet, and S. S. Beauchemin. Performance of optical flow techniques. *International Journal of Computer Vision*, 12(1):43–77, 1994.

[3] D. P. Bertsekas. *Nonlinear Programming*. Athena Scientific, Belmont, MA, 1995. 2nd edition 1999.

[4] M. J. Black and P. Anandan. The robust estimation of multiple motions: Parametric and piecewise-smooth flow fields. *Computer Vision and Image Understanding*, 63(1):75–104, Jan. 1996.

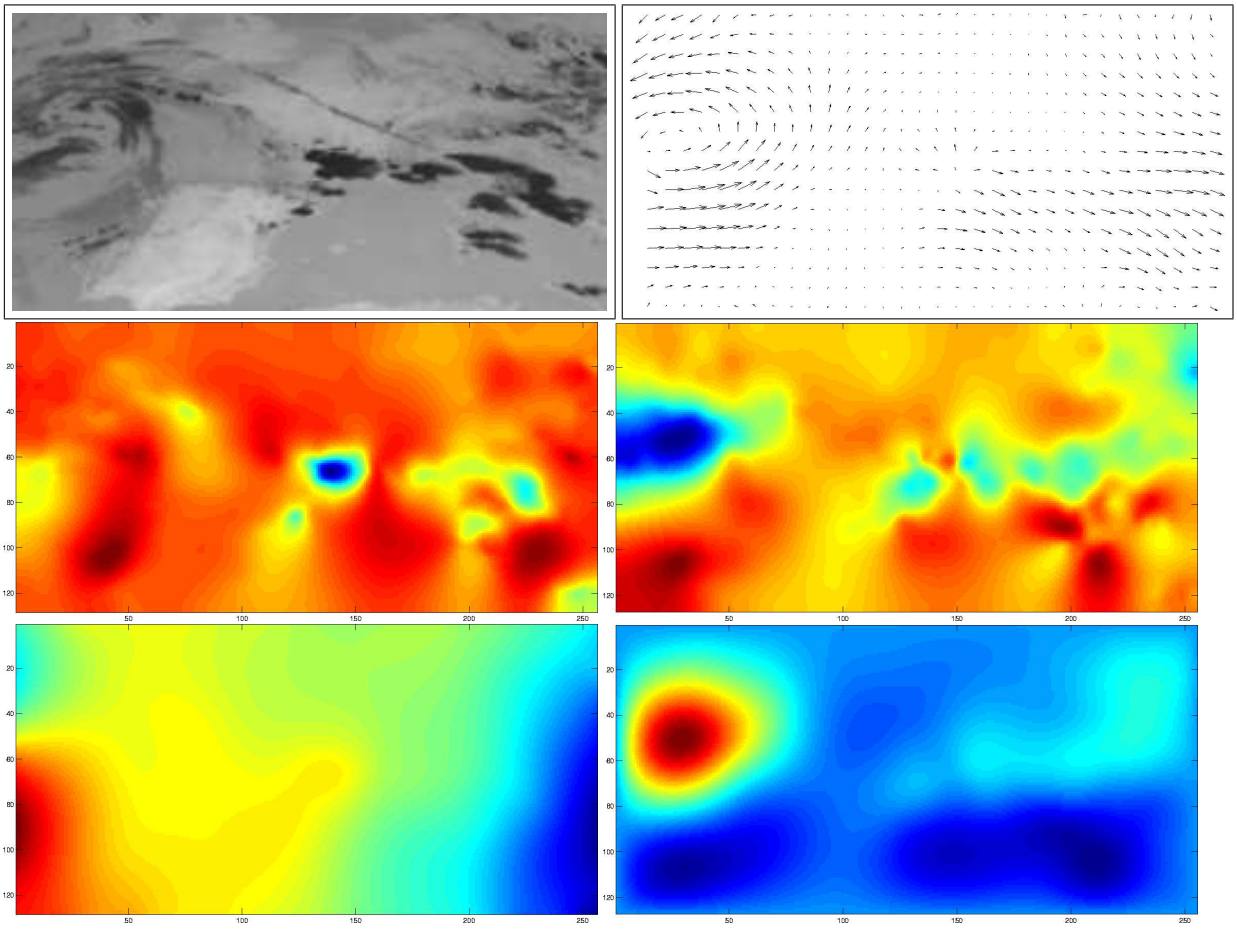

Figure 6: **Top** Image I with the restored flow field u. **Middle Left** The divergence field of u. **Middle Right** The curl field of u. **Bottom Left** The potential field $\psi(\Omega)$. **Bottom Right** The potential field $\phi(\Omega)$. As in the previous figure, the potential functions provide a useful representation of qualitative properties of the flow.

[5] P. Bochev and M. Shashkov. Constrained interpolation (remap) of divergence-free fields, la-ur-03-7903. *J. Comput. Phys.*, 2003.

[6] T. Corpetti, D. Heitz, G. Arroyo, É. Mémin, and A. Santa-Cruz. Fluid experimental flow estimation based on an optical-flow scheme. *Experiments in Fluids*, 40:80–97, 2006.

[7] T. Corpetti, É. Mémin, and P. Pérez. Dense estimation of fluid flows. *IEEE Trans. Pattern Anal. Machine Intell.*, 24(3):365 –380, 2002.

[8] T. Corpetti, É. Mémin, and P. Pérez. Extraction of singular points from dense motion fields: an analytic approach. *J. of Math. Imag. Vision*, 19(3):175–198, 2003.

[9] V. Girault and P.-A. Raviart. Finite element methods for navier-stokes equations. *Springer*, 1986.

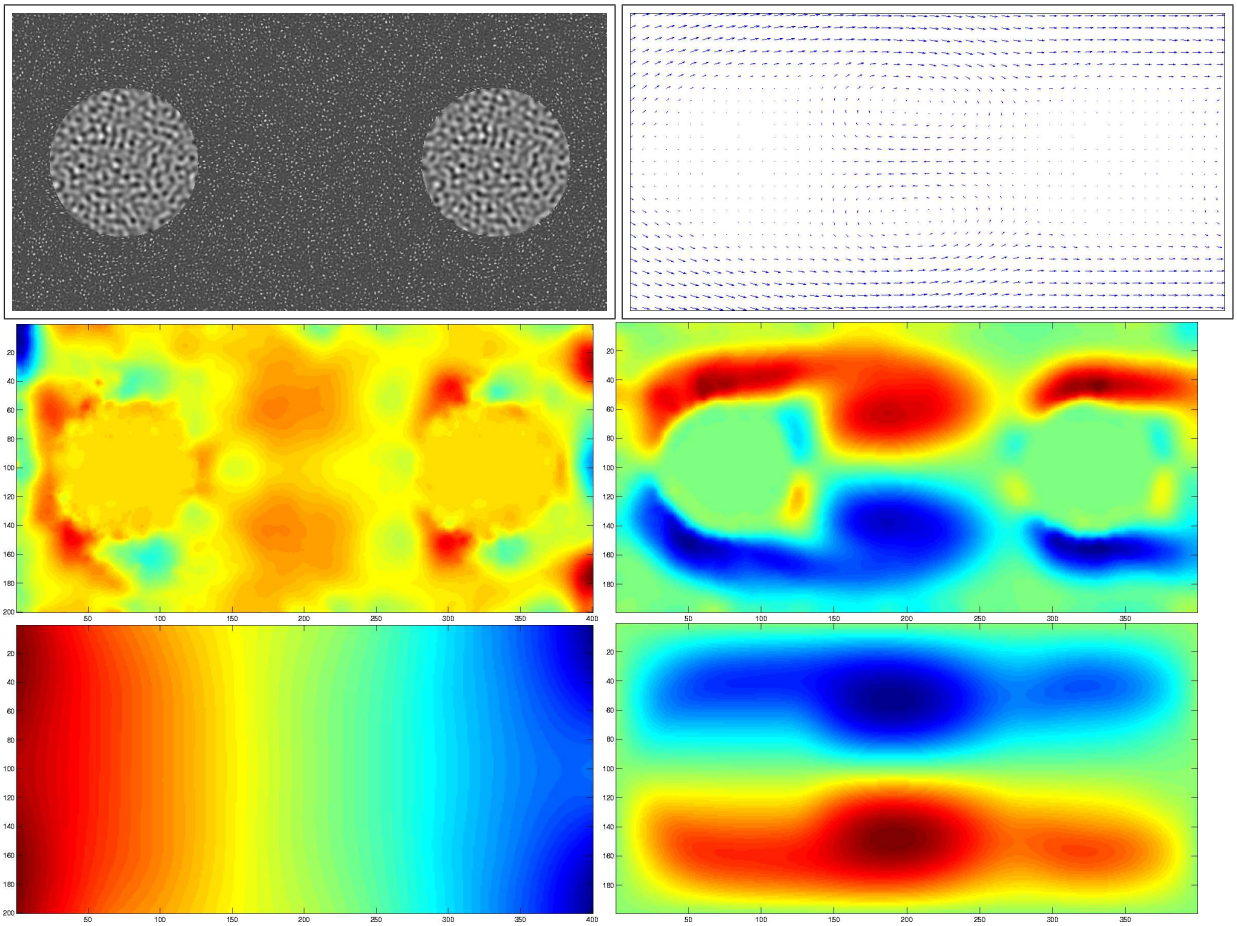

Figure 7: **Top** Image I with the restored flow field u. **Middle Left** The divergence field of u. **Middle Right** The curl field of u. **Bottom Left** The potential field $\psi(\Omega)$. **Bottom Right** The potential field $\phi(\Omega)$. Tow potential fields ψ and ϕ are not zero at the area of two cylinders even if its resulting flow dissappears in these domains. The divergence and curl fields provide clear flow information around two cylinders.

[10] S. Gupta and J. Prince. Stochastic models for div-curl optical flow methods. *Signal Proc. Letters*, 3(2):32–34, 1996.

[11] J. M. Hyman and M. J. Shashkov. Adjoint operators for the natural discretizations of the divergence, gradient and curl on logically rectangular grids. *Appl. Numer. Math.*, 25(4):413–442, 1997.

[12] J. M. Hyman and M. J. Shashkov. Natural discretizations for the divergence, gradient, and curl on logically rectangular grids. *Comput. Math. Appl.*, 33(4):81–104, 1997.

[13] J. M. Hyman and M. J. Shashkov. The orthogonal decomposition theorems for mimetic finite difference methods. *SIAM J. Numer. Anal.*, 36(3):788–818 (electronic), 1999.

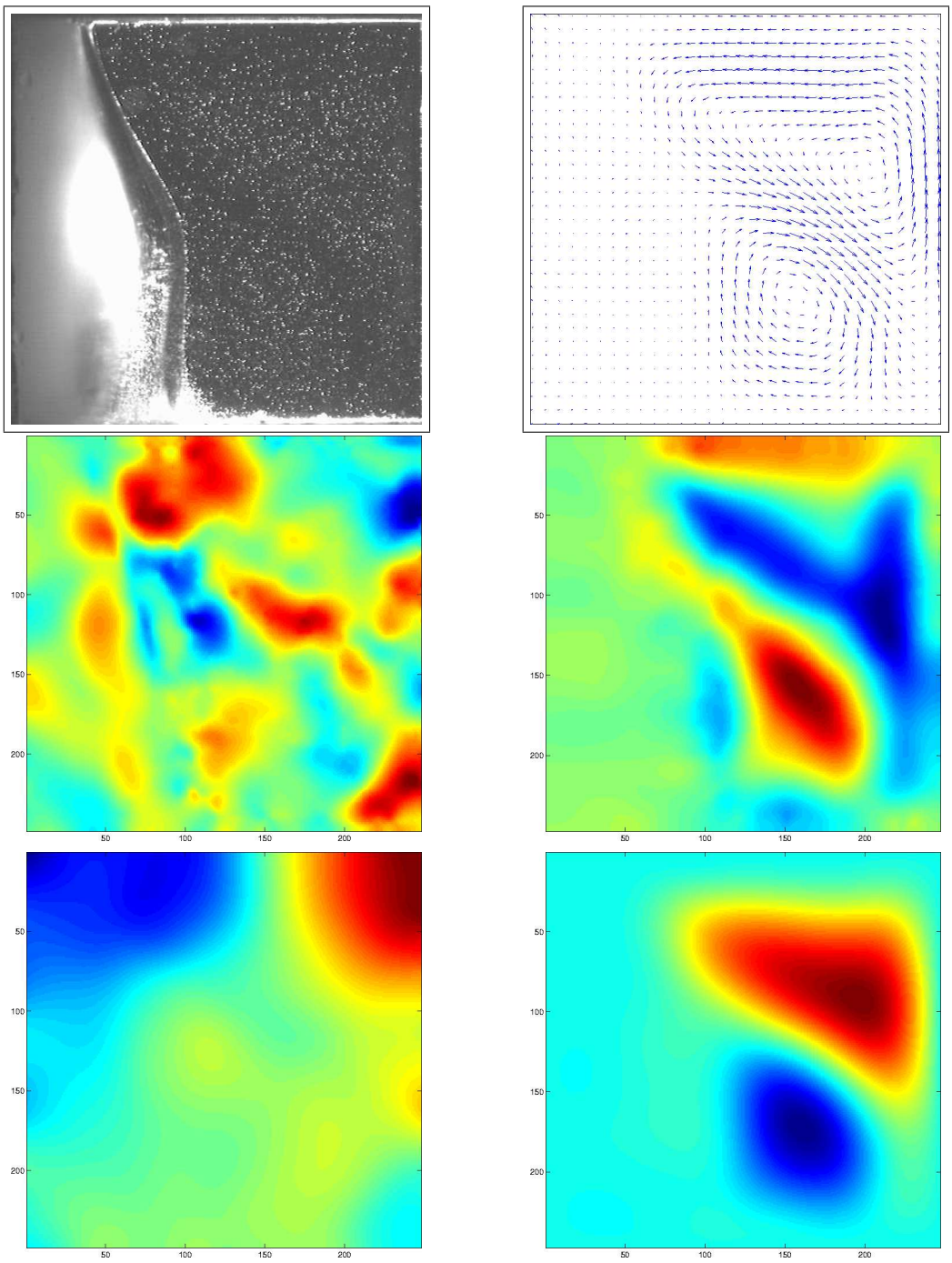

Figure 8: **Top** Image I with the restored flow field u. **Middle Left** The divergence field of u. **Middle Right** The curl field of u. **Bottom Left** The potential field $\psi(\Omega)$. **Bottom Right** The potential field $\phi(\Omega)$. The graphs of potential functions provide a useful representation of qualitative properties of the flow.

[14] T. Kohlberger, E. Mémin, and C. Schnörr. Variational dense motion estimation using the helmholtz decomposition. In L.D. Griffin and M. Lillholm, editors, *Scale Space Methods in Computer Vision*, volume 2695 of *LNCS*, pages 432–448. Springer, 2003.

[15] P. Ruhnau, T. Kohlberger, H. Nobach, and C. Schnörr. Variational optical flow estimation for particle image velocimetry. *Experiments in Fluids*, 38:21–32, 2005.

[16] Y. Saad. *Iterative methods for sparse linear systems*. Society for Industrial and Applied Mathematics, Philadelphia, PA, second edition, 2003.

[17] D. Suter. Motion estimation and vector splines. In *Proceedings of the Conference on Computer Vision and Pattern Recognition*, pages 939–942, Los Alamitos, CA, USA, June 1994. IEEE Computer Society Press.

[18] X.-C. Tai and M. Espedal. Rate of convergence of some space decomposition methods for linear and nonlinear problems. *SIAM J. Numer. Anal.*, 35(4):1558–1570 (electronic), 1998.

[19] X.-C. Tai and P. Tseng. Convergence rate analysis of an asynchronous space decomposition method for convex minimization. *Math. Comp.*, 71(239):1105–1135 (electronic), 2002.

[20] X.-C. Tai and J.-C. Xu. Subspace correction methods for convex optimization problems. In *Eleventh International Conference on Domain Decomposition Methods (London, 1998)*, pages 130–139 (electronic). DDM.org, Augsburg, 1999.

[21] X.-C. Tai and J.-C. Xu. Global and uniform convergence of subspace correction methods for some convex optimization problems. *Math. Comp.*, 71(237):105–124 (electronic), 2002.

[22] G. Tóth and P. L. Roe. Divergence- and curl-preserving prolongation and restriction formulas. *J. Comput. Phys.*, 180(2):736–750, 2002.

[23] J. Xu. Iterative methods by space decomposition and subspace correction: A unifying approach. *SIAM Review*, 34:581–613, 1992.

[24] J.-C. Xu. *Theory of Multilevel Methods*. PhD thesis, Cornell University, May 1989.

[25] J. Yuan, P. Ruhnau, E. Mémin, and C. Schnörr. Discrete orthogonal decomposition and variational fluid flow estimation. In *Scale-Space 2005*, volume 3459, pages 267–278. Springer, 2005.